East European Journal of Physics. 3. 158-167 (2025)
DOI:10.26565/2312-4334-2025-3-14 ISSN 2312-4334

MHD HYBRID NANOFLUIDS FLOW THROUGH POROUS STRETCHING SURFACEIN THE PRESENCE OF THERMAL RADIATION AND CHEMICAL REACTION

Gladys Tharapatla[a], Vijaya Lakshmi Garishe[b], N. Vijaya[c], Sridhar Wuriti[c], G.V.R. Reddy[c]*
[a]*Department H&S, Methodist College of Engineering and Technology, Bogulkunta, Abids, Hyderabad, Telangana 500001, India*
[b]*Department of Mathematics, MGIT, Gandipet, Hyderabad, Telangana, India-500075*
[c]*Department of Mathematics, Koneru Lakshmaiah Education Foundation, Vaddeswaram, India-522302*
Corresponding Author E-mail: gvrr1976@kluniversity.in
Received June 8, 2025; revised August 2, 2925; accepted August 11, 2025

This study investigates the convective transport of heat and mass in a magnetohydrodynamic (MHD) nanofluid flow over a permeable, electrically actuated stretching surface embedded in a porous medium. The analysis incorporates key physical effects including thermal radiation, heat generation, viscosity dissipation, and chemical reactions. The governing equations are formulated to account for the influence of porosity, magnetic fields, thermal and concentration gradients, as well as chemical kinetics. Special attention is given to the control of nanoparticle volume fraction at the boundary interface. Two nanofluid models – Copper–Water (Cu–H_2O) and Aluminum Oxide–Water (Al_2O_3–H_2O)—are considered to assess thermal performance. The nonlinear boundary value problem is solved numerically using a shooting technique combined with a fourth-order Runge–Kutta method. The results show excellent agreement with previously published data, validating the accuracy and robustness of the present model. These findings have potential applications in advanced heat transfer systems, such as cooling technologies and materials processing.
Keywords: *Hybrid nanofluids; MHD; Porous media; Thermal radiation; Skin-friction*
PACS: 47.65.-d, 47.56.+r, 44.40.+a, 66.20.-d, 47.85.mb

Nomenclature

Symbol	Description	Unit			
u, v	Velocity components in x- and y-directions	m/s	D_B	Brownian diffusion coefficient	m^2/s
ψ	Stream function	m^2/s	D_T	Thermophoretic diffusion coefficient	kg/(m·s)
T, T_w, T_∞	Temperature, wall temperature, ambient temperature	K	K_0	Chemical reaction rate constant	s^{-1}
C, C_w, C_∞	Concentration, wall concentration, ambient concentration	kg/m^3	M	Magnetic field parameter	–
μ_{nf}, μ_f	Dynamic viscosity of nanofluid/base fluid	Pa·s	K_1	Porosity parameter	–
ρ_{nf}, ρ_f, ρ_s	Density of nanofluid, base fluid, solid particles	kg/m^3	R	Radiation parameter	–
$(\rho c_p)_{nf}$, $(\rho cp)_f$, $(\rho cp)_s$	Heat capacity of nanofluid, base fluid, solid particles	$J/(m^3·K)$	Pr	Prandtl number	–
k_{nf}, k_f, k_s	Thermal conductivity of nanofluid, base fluid, solid particles	W/(m·K)	Q	Heat source/sink parameter	–
α_{nf}	Thermal diffusivity of nanofluid	m^2/s	Ec	Eckert number	–
ν_f	Kinematic viscosity of base fluid	m^2/s	Sc	Schmidt number	–
η	Similarity variable (dimensionless)	–	Kr	Chemical reaction parameter	–
f(η)	Dimensionless stream function	–	Sr	Soret number	–
θ(η)	Dimensionless temperature	–	φ	Nanoparticle volume fraction	–
φ(η)	Dimensionless concentration	–	ω	Frequency parameter	s^{-1}
σ	Electrical conductivity	S/m	a	Stretching rate constant	s^{-1}
B_0	Magnetic field strength	T	n, m	Surface concentration/temperature gradient indices	–
K	Permeability of porous medium	m^2	f', f'', f'''	First, second, third derivatives of f(η)	–
Q_0	Volumetric heat generation coefficient	W/m^3	θ', θ''	Derivatives of θ(η)	–
q_r	Radiative heat flux	W/m^2	φ', φ''	Derivatives of φ(η)	–
σ*	Stefan–Boltzmann constant	$W/(m^2·K^4)$	ω_1, ω_2, ω_3, ω_4	Non-dimensional grouped parameters	–
K*	Rosseland mean absorption coefficient	m^{-1}			

Cite as: G. Tharapatla, V.L. Garishe, N. Vijaya, S. Wuriti, G.V.R. Reddy, East Eur. J. Phys. 3, 158 (2025), https://doi.org/10.26565/2312-4334-2025-3-14

1. INTRODUCTION

The examination of nanofluids has gotten a considerable sum of consideration in modern scholastic talk. Usually due to the reality that nanofluids have made strides warm properties in differentiate to customary liquids. Nanofluids are a novel category of liquids that are characterised by the nearness of nanoparticles that are suspended inside a substrate liquid. As a result of the extraordinary warm exchange capabilities that they have, they have risen as a potential choice for a huge assortment of mechanical applications. The marvels of boundary layer stream and warm exchange over extended surfaces are basic components of an assortment of building forms. These operations incorporate the expulsion of polymer sheets, strengthening, gem arrangement forms, metal turning, and hot rolling. It was Crane [1] who played a noteworthy part within the starting stages of the examination of stream flow past a extending plate. Hence, a expansive number of analysts have examined the stream and warm exchange characteristics of a assortment of liquids over extended surfaces. The stream of a nanofluid by means of a extended sheet was examined by Khan and Pop [2], who carried out an examination into the boundary layer stream. In his consider [3], Abd El-Aziz examined the impacts of warm dissemination and dissemination thermo on the combined warm and mass exchange wonders that are related with Three-dimensional free flow of water and magnetism over a transparent, long surface, along with rays. A ponder was conducted by Hady and colleagues [4] to assess the impact that radiation has on the gooey stream of a nanofluid and the warm exchange that happens over A sheet with a nonlinear extension. The insecure boundary-layer stream and warm exchange elements with their help, Bachok et al. examined the impact of a little fluid across a penetrable stretching/ shrinkable sheet. [5]. In them consider, Rohni and colleagues [6] used Buongiorno's show to examine the stream and warm exchange characteristics that happened over an unsteady contracting sheet that was subjected to suction in a nanofluid. In arrange to clarify the convective transport forms that take put in nanofluids, Buongiorno [7] proposed a show that comprises of two components. Inside the system of a chemical response, Sandhya et al. [8] conducted inquire about to investigate Heat and mass transfer's influence on a magnetohydrodynamic stream that travelled through a porous plate that was tilted. A non-Darcy common convection administration was the subject of an examination by Murthy and Singh [9], who explored the suggestions of gooey scattering. Motsa [10] displayed an interesting ghostly unwinding method for the examination of closeness variable nonlinear boundary layer stream frameworks. This method was created for those frameworks. The components of an a non-New nanofluid flow past an inclined plate that is speeding were examined by Gladys and Reddy [11], who explored the effect of changing consistency and thermal conductivity on the stream elements. Vijaya and Reddy [12] explored the magnetohydrodynamic stream of Casson liquid across a permeability plate that is vertical, while taking into account the effects of radiation, Soret, along with chemical forms. A numerical examination into common convection was completed by Abu-Nada and Oztop [13] inside rectangular walled in areas that were in part warmed and filled with nanofluids to explore the wonder. A demonstrate in which the thickness of concentrated suspensions and arrangements is taken into thought was created by Brinkman [14]. Maxwell Garnett [15] created a conceptual system that gives a clarification for the colouration marvels that are watched in metallic oxide coatings and glasses. The application of nanofluids for the reason of upgrading warm exchange in isolated streams that are experienced in backward-facing steps was examined by Abu-Nada [16]. Beneath the impact of a attractive field, Hamad [17] was able to get an expository arrangement for the common convection stream of a nanofluid over a sheet that was amplifying in a direct method. A think about conducted by Kameswaran and colleagues [18] looked into the hydromagnetic stream of nanofluids that happened as a result of a sheet that was either extended or contracted. The analysts took into consideration the impacts of thickness dissemination and chemical intuitive. The highlights of warm exchange that are associated with a persistent extended surface that's subject to fluctuating temperature conditions were explored by Grubka and Bobba [19]. Rafique et al. [20] conducted an in-depth mathematical analysis concerning the flow behavior of A mixed nanofluid with magnetohydrodynamics (MHD) at play. This hybrid nanofluid, made up of particles and an organizing liquid, demonstrated good performance in a range of slide and gravity situations. In their study, Nisar et al. [21] examined how the process of heat transmission is affected by thermal transit in single-phase nanofluid flow across radially extended disks, showing Because using water and titanium dioxide as a foundation fluid greatly accelerates the process of heat transfer. Patil et al. [22] conducted a thorough examination of the interactions of magnetized bioconvective micropolar nanofluid as it flowed across a wedge, while also factoring in the role of oxytactic microorganisms. The investigation conducted by Rawat and others [23] focused on how non-homogeneous thermal sources and sinks react to nanoparticle aggregation to change the flow properties of a fluid with a wedge-like shape composed of titania and ethylene glycol. Umavathi [24] focused their investigation on the movement of a micropolar tiny fluids that conducts electricity via a wedge shape while accounting for the effects of ion and Hall winds and a sink or source of heat.

The primary objective of this endeavour is to delve into the flow conundrum of a hybrid nano-fluid comprising Al_2O_3+Cu paired with the base fluid H2O through the lens of the Maxwell fluid model. Intertwined equations of momentum, energy, and mass concentration alongside the influences of Lorentz force, chemical reactions, and the impact of Soret term are considered. A porous plate that stretches linearly and is nestled within porous media is taken into account. Nanoparticles of cylindrical forms are successfully created. In the subsequent sections, the intricacies of modeling and the simulation process are elaborated upon in detail.

2. MATHEMATICAL FORMULATION

We consider two-dimensional steady-state boundary layer flow of an incompressible nanofluid gliding over a permeable stretching sheet, merging the phenomena of thermal and mass transport. The coordinate framework is

established such that its origin resides at the juncture where the sheet initiates its stretching, with the x-axis gracefully tracing along the stretching surface while the y-axis stands perpendicular to it. It is presumed that the externally imposed magnetic field reigns supreme over electromagnetic influences, thereby diminishing the significance of the induced magnetic field, the corresponding electric field, and the field resulting from charge separation to mere whispers. Moreover, the effects of chemical reactions, nanoparticle clustering, and sedimentation are purposefully set aside in this inquiry to home in on the fundamental transport mechanisms. The nanofluid we examine is a remarkable concoction of copper and alumina (Al_2O_3) nanoparticles, elegantly suspended in a water-based medium, where both the fluid and the nanoparticles are believed to exist in thermal harmony—indicating a seamless connection between the phases. The governing equations of the boundary layer—encompassing continuity, momentum, energy, and concentration—are articulated in dimensional form as articulated by Gladys et al. [11], integrating influences such as Brownian motion, thermophoresis, thermal radiation, chemical reactions, and heat sources/sinks.

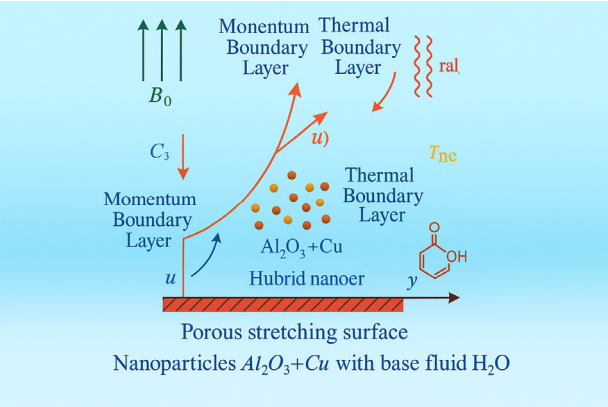

Figure 1. Physical model of the problem

The previously mentioned premises are essential for the definition of these conditions.

$$\frac{\partial u}{\partial x}+\frac{\partial v}{\partial y}=0, \tag{1}$$

$$u\frac{\partial u}{\partial x}+v\frac{\partial u}{\partial y}=\frac{\mu_{nf}}{\rho_{nf}}\frac{\partial^2 u}{\partial y^2}-\left\{\frac{\mu_{nf}}{\rho_{nf}}\frac{1}{K}+\frac{\sigma B_0^2}{\rho_{nf}}\right\}u, \tag{2}$$

$$u\frac{\partial T}{\partial x}+v\frac{\partial T}{\partial y}=\alpha_{nf}\frac{\partial^2 T}{\partial y^2}+\frac{Q_0}{(\rho c_p)_{nf}}(T-T_\infty)+\frac{1}{(\rho c_p)_{nf}}\frac{16\sigma^* T_\infty^3}{3K^*}\frac{\partial^2 T}{\partial^2 y}+\frac{\mu_{nf}}{((\rho c_p)_{nf}}\left(\frac{\partial u}{\partial y}\right)^2 \tag{3}$$

$$u\frac{\partial C}{\partial x}+v\frac{\partial C}{\partial y}=D_B\frac{\partial^2 C}{\partial y^2}+\frac{D_T}{T_\infty}\frac{\partial^2 T}{\partial y^2}-K_0(C-C_\infty). \tag{4}$$

The following are the requirements for the conditions governing the boundaries for equations (1) through (4):

$$\begin{cases} \mathrm{u}=ax, v=0, T=T_{\mathrm{w}}(x)=T_\infty+m\left(\frac{x}{\omega}\right)^2, C=C_{\mathrm{w}}(x)=C_\infty+n\left(\frac{x}{\omega}\right)^2 & \text{at } y=0 \\ u\to 0, T\to T_\infty, C\to C_\infty & \text{as } y\to\infty \end{cases} \tag{5}$$

where ω is the defining frequency and n, m, and an all integers, and a > 0.
Here q_r is the heat flow from radiation. [12] given by

$$q_r=-\frac{4\sigma^*}{3K^*}\frac{\partial T^4}{\partial y}, \tag{6}$$

where K* is the Rosseland average absorption factor and σ* is the Stefen-Boltzmann constant. The temperature was fluctuation T^4 is shown using an expanded version of the Taylor series. Ignoring more complex phrases and extending T^4 around T_∞ results in:

$$T^4=4T_\infty^3-3T_\infty^4. \tag{7}$$

Brinkman provided the nanofluid's efficient variable viscosity [14] as

$$\mu_{nf}=\frac{\mu_f}{(1-\phi)^{2.5}}, \tag{8}$$

where ϕ and μ_f represents the movement of the base fluid with the solid volume fraction of tiny particles, respectively. The heat impedance and warmth conductivity of nanofluids, especially those limited to spherical nanoparticles, are estimated using the Max-Garnett model (see Maxwell Garnett [15]) in equations (1) through (4).

$$\begin{gathered}\left(\rho c_p\right)_{nf}=(1-\phi)\left(\rho c_p\right)_f+\phi\left(\rho c_p\right)_s, \\ \rho_{nf}=(1-\phi)\rho_f+\phi\rho_s, v_{nf}=\frac{\mu_{nf}}{\rho_{nf}}, \\ \alpha_{nf}=\frac{k_{nf}}{\left(\rho c_p\right)_{nf}}, k_{nf}=k_f\left[\frac{(k_s+k_f)-2\phi(k_f-k_s)}{(k_s+k_f)+\phi(k_f-k_s)}\right],\end{gathered} \tag{9}$$

where $v_{nf}, \rho_{nf}, \left(\rho c_p\right)_{nf}, k_{nf}, k_f, k_s, \rho_s, \left(\rho c_p\right)_f, \left(\rho c_p\right)_s$. These include the physical viscosity of nanofluids, electrical conductivity properties, particular warmth capacity of the temperature transmission of the initial fluid, the thermal conductivity of the solid individuals, the density of the particles, the heat transmission of the tiny fluids, and the solid constituents, base fluid's heat capacity, and effective heat capacity caused by tiny particles, in that order.
It introduces a function of streams ψ(x,y) to fulfil the continuity equation (1) in such a way that:

$$u=\frac{\partial\psi}{\partial y}, v=-\frac{\partial\psi}{\partial x}. \tag{10}$$

Introducing the non-dimensional variables listed below,

$$\begin{gathered}\psi=\left[av_f\right]^{\frac{1}{2}}xf(\eta), u=axf'(\eta), v=-\left(av_f\right)f(\eta), \\ \theta(\eta)=\frac{T-T_\infty}{T_w-T_\infty}, \varphi(\eta)=\frac{C-C_\infty}{C_w-C_\infty}, \eta=\left[\frac{a}{v_f}\right]^{\frac{1}{2}}y\end{gathered} \tag{11}$$

where θ(η) is the undefined temperature, f(η) is the dimensionless flow function, is the undetermined focus, while the similarity variables are denoted by η. The following two-point border value dilemma is created by combining equations (6) to (11) with the fundamental equations (2), (3), and (4) as well as the circumstances of the boundaries (5):

$$f'''+\omega_1\left[ff''-f'^2-\frac{1}{\omega_2}Mf'\right]-K_1f'=0, \tag{12}$$

$$\left(1+\frac{4R}{3}\right)\theta''+\omega_3\left[f\theta'-2f'\theta+Q\theta+\frac{E_c}{\omega_4}f''^2\right]=0, \tag{13}$$

$$\varphi''+Sc(f\varphi'-2f'\varphi+Kr\varphi)+Sr\theta''=0. \tag{14}$$

based on border requirements.

$$\begin{cases}f=0, f'=1, \theta=1, \varphi=1 & at\ \eta=0\ and \\ f'\to 0, \theta\to 0, \varphi\to 0 & as\ \eta\to\infty\ .\end{cases} \tag{15}$$

Primes indicate specialization with respect to η, while the base fluid's thermal diffusion and velocity of motion are represented by η, $\alpha_f=\left(\frac{k_f}{\rho C_p}\right)$ and $\nu_f=\frac{\mu_f}{\rho_f}$ respectively. Additional non-dimensional characteristics that show up in formulas (12) to (15) are $M, K_1, R, Pr, Q, E_c, Sc, Kr$ and Sr indicate the parameters for heat generation, Schmidt, Eckert, scaled chemical reaction, magnetized, porous material, Soret, Prandtl, and heat radiation values. The mathematical definition of these parameters is

$$\begin{gathered}M=\frac{\sigma B_0^2}{a\rho_f}, K_1=\frac{v_f}{ak}, R=\frac{4\sigma^*T_\infty^3}{k^*k_{nf}}, Sc=\frac{v_f}{D} \\ \Pr=\frac{v_f\left(\rho c_p\right)_f}{k_f}, Q=\frac{Q_0}{a\left(\rho c_p\right)_{nf}}, Kr=\frac{K_0}{a}\ , \\ E_c=\frac{u_w^2}{(T_w-T_\infty)\left(c_p\right)_f}, Sr=\frac{D_1(T_w-T_\infty)}{D(C_w-C_\infty)}.\end{gathered} \tag{16}$$

The definition of the nanoparticle volume fractions ϕ_1 and ϕ_2 is.

$$\begin{gathered}\omega_1=(1-\phi)^{2.5}\left[1-\phi+\phi\left(\frac{\rho_s}{\rho_f}\right)\right], \omega_2=1-\phi+\phi\frac{(\rho_s)}{(\rho_f)}, \\ \omega_3=1-\phi+\phi\frac{\left(\rho c_p\right)_s}{\left(\rho c_p\right)_f}, \omega_4=(1-\phi)^{2.5}\left[1-\phi+\phi\frac{\left(\rho c_p\right)_s}{\left(\rho c_p\right)_f}\right].\end{gathered} \tag{17}$$

3. SKIN FRICTION, HEAT AND MASS TRANSFER COEFFICIENTS

The mass transfer, wall heat, and surface drag ratios are described by the rate of skin friction C_f, Sherwood's regional value Sh_x, and the Nusselt code in the area Nu_x, respectively quantities of engineering relevance.
The definition for the shear strain τw at a structure's surface is.

$$\tau_w=-\mu_{nf}\left(\frac{\partial u}{\partial y}\right)_{y=0}=-\frac{1}{(1-\phi)^{2.5}}\rho_f\sqrt{v_fa^3}xf''(0), \tag{18}$$

where μ_{nf} is the viscosity coefficient. The rate of skin friction is determined as.

$$C_{fx} = \frac{2\tau_w}{\rho_f U_w^2}, \tag{19}$$

and using equation (18) in (19) we obtained

$$0.5(1-\phi)^{2.5} C_{fx} = -\mathrm{Re}_x^{-\frac{1}{2}} f''(0). \tag{20}$$

The definition of rate of heat transfer at the level of a wall flux is.

$$q_w = -k_{nf}\left(\frac{\partial T}{\partial y}\right)_{y=0} = -k_{nf}\frac{(T_w - T_\infty)}{x}\sqrt{\frac{U_w x}{v_f}}\theta'(0), \tag{21}$$

where k_{nf} is the nanofluids thermal resistance. The definition of the localized Nusselt value is.

$$Nu_x = \frac{x q_w}{k_f(T_w - T_\infty)}. \tag{22}$$

Equation (21) multiplied by equation (22) yields the wall heat transfer rate without measurements.

$$\left(\frac{k_f}{k_{nf}}\right) Nu_x = -Re_x^{0.5}\theta'(0). \tag{23}$$

The definition of the borders appears, the volume of flow is

$$q_m = -D\left(\frac{\partial C}{\partial y}\right)_{y=0} = -DQ\left(\frac{x}{\omega}\right)^2\sqrt{\frac{a}{v_f}}\varphi'(0), \tag{24}$$

and the local Sherwood code is obtained as.

$$Sh_x = \frac{x q_m}{D(C_w - C_\infty)}. \tag{25}$$

The rate of mass transfer across indeterminate walls from (24) and (25) is obtained as

$$Sh_x = -\mathrm{Re}_x^{\frac{1}{2}}\varphi'(0), \tag{26}$$

where Re_x, which stands for the regional Reynolds value is explained as follows:

$$Re_x = \frac{x u_w}{v_f}$$

4. METHOD OF SOLUTION

The mathematical expressions that are symbolized by the numbers (12) to (14) display a significant degree of non-linearity, which has the effect of making the process of deriving explicit solutions more difficult. Since this is the case, the resolutions of these mathematical constructs, in addition to the boundary conditions that were described in (15), were achieved by numerical methods that utilized combining the fourth-order Runge-Kutta process with the firing method (Figure 1).

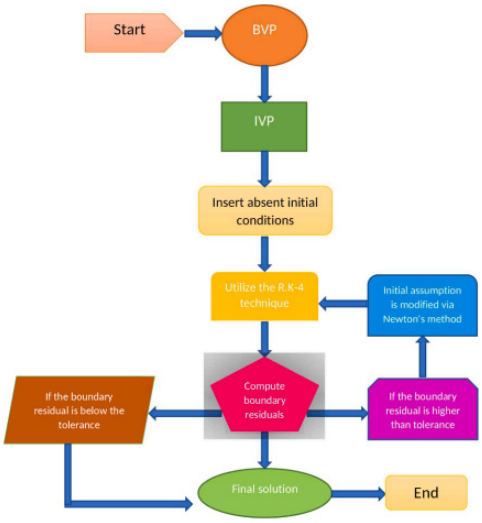

Figure 1. Model flow diagram (RK-Method).

5. RESULTS AND DISCUSSION

Table 1 may be an introduction of the thermophysical chattels of the nanofluids that were utilized into the numerical recreations. Broad calculations have been carried out in arrange to set up the profiles of many physical characteristics, including touching the skin, the adjacent null number, the local Forest amount, and the profiles of velocity, temperature, and concentration., counting ϕ, M, K1, R, Pr, Sc, Q, Ec, Kr, and Sr.

Table 1. Thermal physical properties

Physical Properties	Base fluid (H_2O)	Copper (Cu)	Alumina (Al_2O_3)
C_p(J/kgK)	4179	385	765
ρ(Kg/m^3)	997.1	8933	3970
k(W/mK)	0.613	401	40

These figures, which expand from 2 to 11, layout the impacts that physical parameters have on a combination of fluid lively characteristics. A diagram of how the alluring parameter M impacts the speed profile of the nanofluids Cu-water and Al_2O_3-water can be found in Figure 2. Extending the alluring parameter M comes almost in a drop inside the nanofluid speed characteristics of Cu-water and Al_2O_3-water. The justification for the frequent use of a transversal enticing field on a fluid that conducts control comes almost inside the arrangement of an obstructing Lorenz drive. This drive moderates down the development of the flow rate decreases when the fluid passes through the topmost layer. In any event, this results in a rise in both heat and concentrations of solutes.

The connection between the porous media parameter K_1 and the speed of nanofluids composed of copper water and Al_2O_3 water is laid out in Figure 3. An increase inside the porous medium parameter K_1 comes almost in a drop inside the speed profiles of both of the nanofluids. The figure illustrates that the Al_2O_3-water nanofluids speed pattern is essentially greater than the Nanofluids of Cu-water.

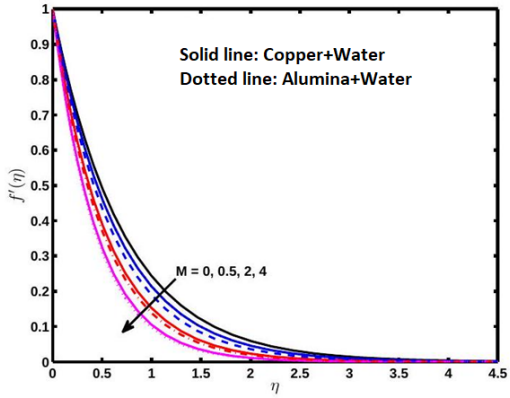

Figure 2. Effect of magnetic parameter M on the velocity profiles

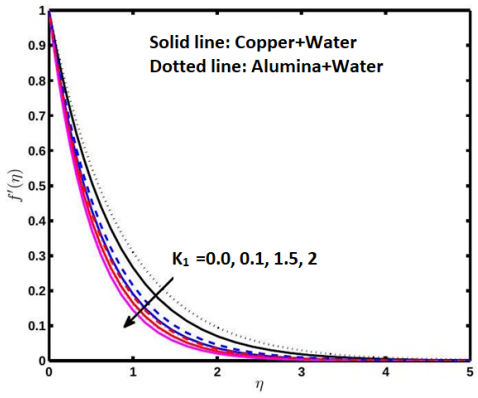

Figure 3. Effect of the porous medium parameter K_1 on the velocity profiles

The impact of nanoparticle volume splitting on temperature, velocity, and concentrations profiles is seen in Figures 4 through 6 independently for a Cu-water tiny fluids and an Al_2O_3-water tiny fluids. These figures appear the impacts of the nanoparticle volume division. Extending the nanoparticle volume division comes around in a reduce inside the velocity of the Al_2O_3-water nanofluid is faster than that of the Cu-water tiny fluids. Figure 5 makes it generously clear that growing the increase in the heated permeability of the small fluid brought on by the particle expansion rate causes the heated boundary layer to thicken.

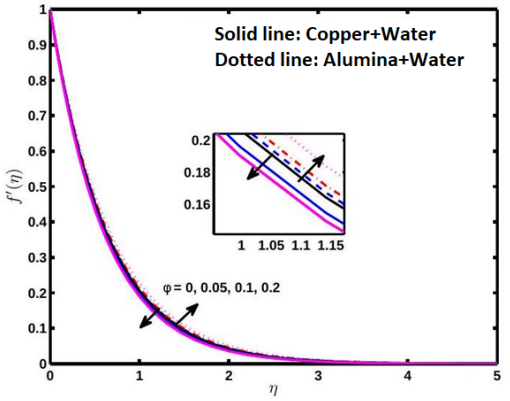

Figure 4. Effect of various nanoparticle values fraction ϕ on velocity profiles

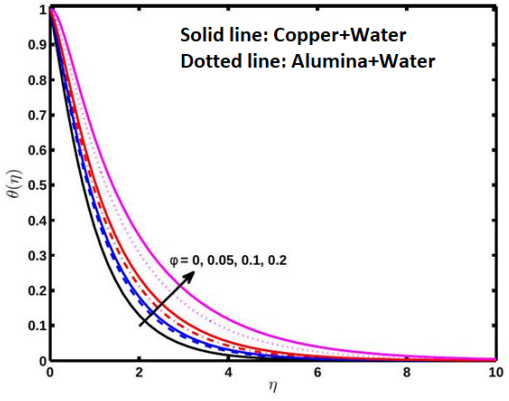

Figure 5. Effect of various nanoparticle values fraction ϕ on temperature profiles

The temperature profile is shown to form when the nanoparticle size division values rise, as illustrated in Figure 6. Because of the reality that copper water may be a strong conductor of both warm and control, it has additionally been showed up that the temperature spread in a nanofluid composed of copper water is more noticeable than that of a nanofluid composed of aluminum oxide water. Figure 6 traces that the concentration profile of Al_2O_3-water nanofluid decreases as the total percentage of nanoparticles rises; nonetheless, it still needs Cu-water tiny fluids.

The temperature profile's response to the warm period parameter Q is portrayed in Figure 7, which portrays the circumstance including nanofluids composed of Al_2O_3-water and Cu-water. We found that as the warm producing parameter Q rose, the thermal profile for both kinds of tiny fluids increased as well. This was seen to be true. According to the findings, the Cu-water nanofluids had a greater temperature than the Al_2O_3-water nanofluids. An increase in the warm conductance of the tiny fluids and a thickening of the warm border layer result from expanding the values of the warmth era parameter Q.

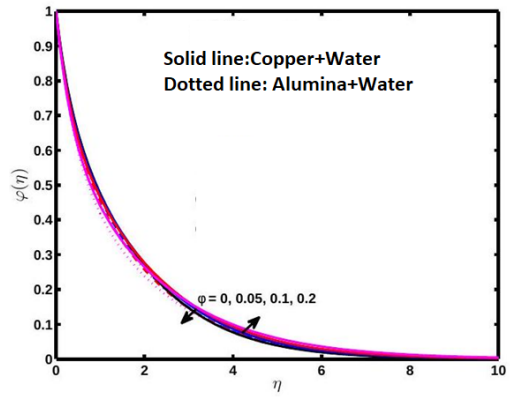

Figure 6. Effect of volume fraction ϕ on the concentration profiles

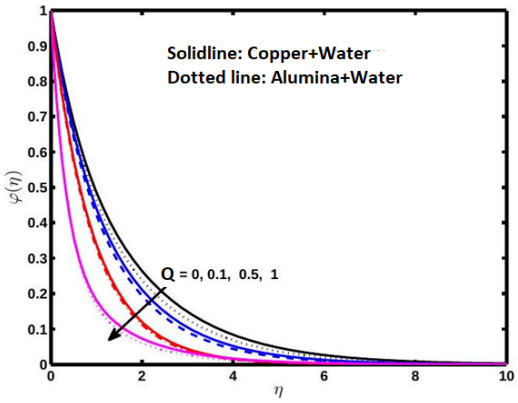

Figure 7. Effect of heat generation parameter Q on the concentration profiles

Figure 8 portrays how the gooey scattering parameter Ec influences the temperature profile for the nanofluids Al_2O_3 and Cu. With an increment in Ec values, it is seen that both nanofluids' temperature profiles rise; this recommends that an increment in Ec impacts the temperature dispersion. Typically, since the liquid locale stores the vitality after it scatters due to thickness and flexible distortion. Cu-water nanofluid shows a more noteworthy temperature profile than Al_2O_3-water nanofluid, it has been watched.

Figure 9 delineates how the warm radiation parameter R influences both nanofluids' temperature distributions. Al_2O_3- and Cu-water nanofluids have higher temperature profiles when the warm radiation Parameter R is expanded. We found that Cu-water nanofluids display bigger temperature increments than Al_2O_3-water nanofluids. The warm irradiation parameter R is what leads to the thickening of the warmer border layer. Consequently, the framework is cooled and the nanofluids can release the warm vitality from the stream zone. Usually exact since a bigger Rosseland estimation causes a bigger temperature profile.

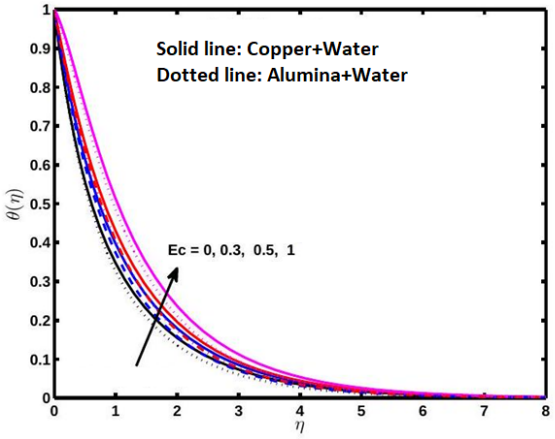

Figure 8. Effect of viscous dissipation parameter E_c on the temperature profiles

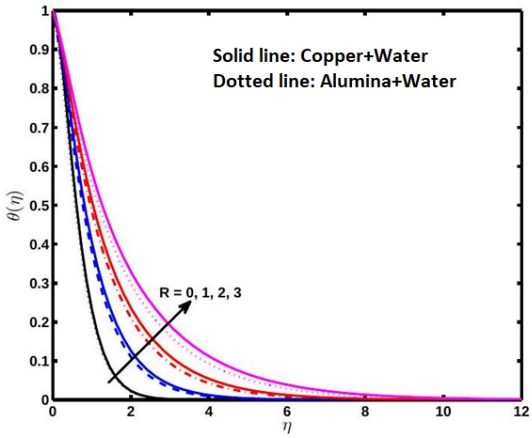

Figure 9. Effect of thermal radiation parameter R on the temperature profiles

Figure 10 appears how for Cu and Al_2O_3 nanofluids, the particle size profile is affected by the Stoner number Sc. Both cases of nanofluids have a lower solutal concentration profile when Sc values are expanded. Cu water nanofluid's concentration profile is seen to extend more than Al_2O_3-water nanofluid's.

Figures 11 and 12 illustrate the effect of two parameters, to be specific the impact of the Soret number Sr and the chemical sensitive variable Kr on the level profiles of the Cu-water and Al_2O_3-water tiny fluids independently.

Distinguish how the biological reaction variable affects the pace and temperature patterns of the nanofluids in the two scenarios does not shift considerably with expanding values of the scale chemical response parameter. Al_2O_3-water nanofluid's solutal concentration profiles in Figure 11 are generally diverse from those of water and copper nanofluids. The solvent content boundary barrier's thickness in both nanofluid scenarios develops as the Soret number Sr increments, as appeared in Figure 12. We found that Al_2O_3-water nanofluid has lower solutal concentration profiles increment than Cu-water nanofluid.

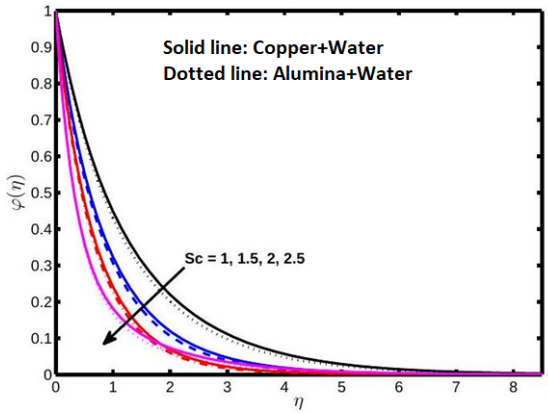

Figure 10. Effect of the Schmidt number Sc on concentration profiles

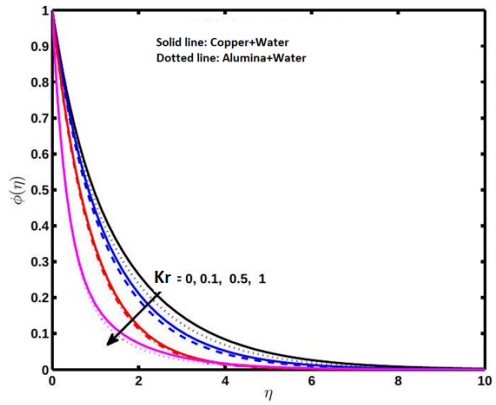

Figure 11. Effect of the chemical reaction parameter Kr on the concentration profiles

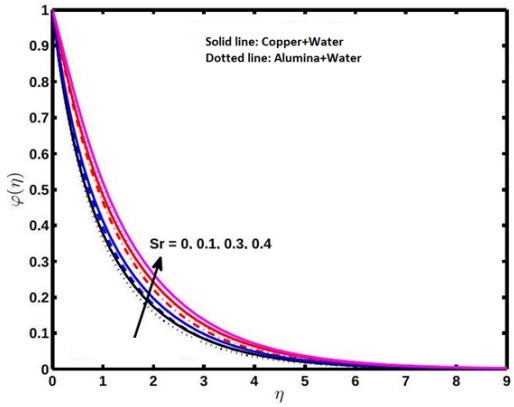

Figure 12. Effect of the Soret number Sr on concentration profiles

Table 2. SRM solutions for f''(0), -θ'(0), and -φ'(0) are compared for various values of Sr, Sc, Q and $Kr \cdot \ \phi = 0.1, E_c = 1, M = 0.5, Sc = 1, Q = 0.02, Pr = 7, K_1 = 1, Kr = 0.08, Sr = 0.2$.

	Cu +water			Al_2O_3 + water		
	$\phi = 0.1, E_c = 1$		$R = 1.5, Pr = 7$		$K_1 = 1.25, M = 0.5$	
Sr	$f''(0)$	$-\theta'(0)$	$-\varphi'(0)$	$f''(0)$	$-\theta'(0)$	$-\varphi'(0)$
0.0	1.67923	0.264822	1.205443	1.543656	0.387837	1.234462
0.1	1.67923	0.264822	1.206502	1.543656	0.387837	1.226048
0.3	1.67923	0.264822	1.208618	1.543656	0.387837	1.209225
0.4	1.67923	0.264822	1.209677	1.543656	0.387837	1.200809
Sc						
0.6	1.67923	0.264822	1.20756	1.543656	0.387837	1.217637
0.7	1.67923	0.264822	1.578602	1.543656	0.387837	1.591183
0.8	1.67923	0.264822	1.89231	1.543656	0.387837	1.906038
0.9	1.67923	0.264822	2.168352	1.543656	0.387837	2.182708
Kr						
0.6	1.67923	0.264822	1.142691	1.543656	0.387837	1.158075
0.7	1.67923	0.264822	1.221807	1.543656	0.387837	1.230985
0.8	1.67923	0.264822	1.441995	1.543656	0.387837	1.442644
0.9	1.67923	0.264822	1.646539	1.543656	0.387837	1.643275

The findings from the numerical exploration shed light on how the Soret number (Sr), the Schmidt number (Sc), and the chemical reaction parameter (Kr) influence the flow, thermal, and concentration boundary layers for Cu–Water and Al_2O_3–Water nanofluids, all while keeping the physical parameters uniform (ϕ = 0.1, Ec = 1, R = 1.5, Pr = 7, K_1 = 1.25,

M = 0.5). It becomes evident that the skin friction coefficient f″(0) and the heat transfer rate −θ′(0) remain steadfast, showing no fluctuations with changes in Sr, Sc, and Kr for both types of nanofluids, indicating that these factors wield a minimal influence on the momentum and thermal boundary layers in this context. Nevertheless, it is noteworthy that the mass transfer rate −ϕ′(0) exhibits a dramatic surge as Sc and Kr are elevated, while Sr demonstrates a more gradual increase. This highlights the crucial significance of Sc and Kr in molding the concentration boundary layer. In a striking contrast, Al_2O_3–Water consistently showcases slightly enhanced heat and mass transfer rates compared to its counterpart, Cu–Water. This suggests that Al_2O_3–Water possesses superior capabilities for thermal and solutal transport, especially when exposed to the effects of heightened Schmidt numbers and chemical reaction rates.

6. CONCLUSION

This study highlights the crucial impact of thermal radiation and heat source/sink effects on the thermo-hydraulic performance of Al_2O_3/water nanofluid and Cu–Al_2O_3/water hybrid nanofluids in the context of advanced energy storage systems. Utilizing the radiation heat flux model and heat source and solving the system through the Runge-Kutta numerical method, the findings reveal that increasing thermal radiation and heat generation parameters significantly enhance temperature distribution and alter fluid flow behavior. The synergistic combination of Cu and Al_2O_3 nanoparticles leads to improved heat transfer efficiency while maintaining thermal and hydrodynamic stability. These outcomes provide a strong computational framework for deploying hybrid nanofluids in sustainable and efficient thermal management applications. The velocity profile decreases with increasing values of the magnetic field parameter.

- The velocity distribution also reduces as the porosity parameter increases.
- The temperature profile increases with higher values of the thermal radiation parameter and the heat source parameter, but shows a decline beyond certain values of the heat source.
- An increase in thermal radiation leads to a further rise in temperature distribution.
- The temperature profile is further enhanced as the nanoparticle volume fraction increases.
- The concentration profile decreases with increasing values of the Schmidt number and the chemical reaction parameter, but increases when the Soret number rises.

ORCID

Gladys Tharapatla, https://orcid.org/0000-0003-4532-9654; **Vijaya Lakshmi Garishe,** https://orcid.org/0000-0001-7210-5678
N. Vijaya, https://orcid.org/0000-0002-6648-1973; **Sridhar Wuriti,** https://orcid.org/0000-0002-0978-1769
G.V.R. Reddy, https://orcid.org/0000-0002-6455-3750

REFERENCES

[1] L.J. Crane, "Flow past a stretching plate," ZAMP. Angew Math. Phys, **21**, 645-647 (1970). https://doi.org/10.1007/BF01587695
[2] W.A. Khan, and I. Pop, "Boundary layer flow of a nanofluid past a stretching sheet," International Journal of Heat and Mass Transfer, **53**, 2477-2483 (2010). https://doi.org/10.1016/j.ijheatmasstransfer.2010.01.032
[3] M. Abd El-Aziz, "Thermal-diffusion and diffusion-thermo effects on combined heat and mass transfer by hydromagnetic three-dimensional free convection over a permeable stretching surface with radiation," Physics Letters, **372**(3), 263-272 (2007). https://doi.org/10.1016/j.physleta.2007.07.015
[4] F.M. Hady, F.S. Ibrahim, S.M. Abdel-Gaied, and R.M. Eid, "Radiation effect on viscous flow of a nanofluid and heat transfer over a nonlinearly stretching sheet," Nanoscale Res. Lett. **7**, 229 (2012). https://doi.org/10.1186/1556-276X-7-229
[5] N. Bachok, A. Ishak, and I. Pop, "Unsteady boundary-layer flow and heat transfer of a nanofluid over a permeable stretching/shrinking sheet," International Journal of Heat and Mass Transfer, **55**, 2102-2109 (2012). https://doi.org/10.1016/j.ijheatmasstransfer.2011.12.013
[6] A.M. Rohni, A.S. Ahmad, and Md.I. Ismail, and I. Pop, "Flow and heat transfer over an unsteady shrinking sheet with suction in a nanofluid using Buongiorno's model," International Communications in Heat and Mass Transfer, **43**, 75-80 (2013). https://doi.org/10.1016/j.icheatmasstransfer.2013.02.001
[7] J. Buongiorno, "Convective transport in nanofluids," ASME Journal of Heat Transfer, **128**, 240-250. https://doi.org/10.1115/1.2150834
[8] A. Sandhya, G.R. Reddy, and G.V.S.R. Deekshitulu, "Heat and mass transfer effects on MHD flow past an inclined porous plate in the presence of chemical reaction," International Journal of Applied Mechanics and Engineering, **25**(3), 86-102 (2020). https://doi.org/10.2478/ijame-2020-0036
[9] P.V. Murthy, and P. Singh, "Effect of viscous dissipation on a non-Darcy natural convection regime," International Journal of Heat and Mass Transfer, **40**, 1251-1260 (1997). https://doi.org/10.1016/S0017-9310(96)00181-0
[10] S.S. Motsa, "A New spectral relaxation method for similarity variable nonlinear boundary layer flow systems," Chemical Engineering Communications, **16**, 23-57 (2013). https://doi.org/10.1155/2014/341964
[11] T. Gladys, and G.R. Reddy, "Contributions of variable viscosity and thermal conductivity on the dynamics of non-Newtonian nanofluids flow past an accelerating vertical plate," Partial Differential Equations in Applied Mathematics, **5**, 100264 (2022). https://doi.org/10.1016/j.padiff.2022.100264
[12] K. Vijaya, and G.V.R. Reddy, "Magnetohydrodynamic Casson fluid flow over a vertical porous plate in the presence of radiation, Soret and chemical reaction effects," Journal of Nanofluids, **8**(6), 1240-1248 (2019). https://doi.org/10.1166/jon.2019.1684
[13] H.F. Oztop, and E. Abu-Nada, "Numerical study of natural convection in partially heated rectangular enclosures filled with nanofluids," International Journal of Heat and Fluid Flow, **29**, 1326-1336 (2008). https://doi.org/10.1016/j.ijheatfluidflow.2008.04.009

[14] H.C. Brinkman, "The viscosity of concentrated suspensions and solution," Journal of Chemical Physics, **20**, 571-581 (1952). https://doi.org/10.1063/1.1700493
[15] J.C.M. Garnett, "Colours in metal glasses and in metallic films," Philosophical Transactions of the Royal Society of London, **203**, 385-420 (1904). https://doi.org/10.1098/rsta.1904.0024
[16] E. Abu-Nada, "Application of nanofluids for heat transfer enhancement of separated flows encountered in a backward facing step," International Journal of Heat and Fluid Flow, **29**, 242-249 (2008). https://doi.org/10.1016/j.ijheatfluidflow.2007.07.001
[17] M.A.A. Hamad, "Analytical solution of natural convection flow of a nanofluid over a linearly stretching sheet in the presence of magnetic field," International Communications in Heat and Mass Transfer, **38**, 487-492 (2011). https://doi.org/10.1016/j.icheatmasstransfer.2010.12.042
[18] P.K. Kameswaran, M. Narayana, P. Sibanda, and P.V. Murthy, "Hydromagnetic nanofluid flow due to a stretching or shrinking sheet with viscous dissipation and chemical reaction effects" International Journal of Heat and Mass Transfer, **55**, 7587–7595 (2012). https://doi.org/10.1016/j.ijheatmasstransfer.2012.07.065
[19] L.G. Grubka, and K.M. Bobba, "Heat transfer characteristics of a continuous stretching surface with variable temperature," The ASME Journal of Heat Transfer, **107**, 248-250 (1985). https://doi.org/10.1115/1.3247387
[20] K. Rafique, Z. Mahmood, and U. Khan, "Mathematical analysis of MHD hybrid nanofluid flow with variable viscosity and slip conditions over a stretching surface," Materials Today Communications, **36**, 106692 (2023). https://doi.org/10.1016/j.mtcomm.2023.106692
[21] S. Nasir, W. Alghamdi, T. Gul, I. Ali, S. Sirisubtawee, and A. Aamir, "Comparative analysis of the hydrothermal features of TiO2 water and ethylene glycol-based nanofluid transportation over a radially stretchable disk," Numerical Heat Transfer, Part B: Fundamentals, **83**(5), 276-291 (2023). https://doi.org/10.1080/10407790.2023.2173343
[22] P.M. Patil, B. Goudar, and E. Momoniat, "Magnetized Bioconvective micropolar nanofluid flow over a wedge in the presence of oxytactic microorganisms," Case Stud. Therm. Eng. **49**, 103284 (2023). https://doi.org/10.1016/j. csite.2023.103284
[23] S.K. Rawat, M. Yaseen, U. Khan, M. Kumar, A. Abdulrahman, S.M. Eldin, S. Elattar, *et al*., "Insight into the significance of nanoparticle aggregation and non-uniform heat source/sink on titania–ethylene glycol nanofluid flow over a wedge," Arab. J. Chem. **16**, 104809 (2023). https://doi.org/10.1016/j.ijheatmasstransfer.2012.07.065
[24] J.C. Umavathi, "Electrically conducting micropolar nanofluid with heat source/sink over a wedge: ion and hall currents," J. Magn. Magn. Mater. **559**, 169548 (2022). https://doi.org/10.1016/j.jmmm.2022.169548

ПОТІК ГІБРИДНОЇ МГД НАНОРІДИНИ ЧЕРЕЗ ПОРИСТУ ПОВЕРХНЮ З РОЗТЯГНЕННЯМ ЗА НАЯВНОСТІ ТЕПЛОВОГО ВИПРОМІНЮВАННЯ ТА ХІМІЧНОЇ РЕАКЦІЇ

Гледіс Тарапатла[a], Віджая Лакшмі Гаріше[b], Н. Віджая[c], Шрідхар Вуріті[c], Г.В.Р. Редді[c]
[a]Кафедра охорони здоров'я та безпеки, Методистський коледж інженерії та технологій, Богулкунта, Абідс, Хайдерабад, Телангана 500001, Індія
[b]Кафедра математики, MGIT, Ганділет, Хайдерабад, Телангана, Індія-500075
[c]Кафедра математики, Освітній фонд Конеру Лакшмаї, Ваддесварам, Індія-522302

Це дослідження вивчає конвективний перенос тепла та маси в магнітогідродинамічному (МГД) потоці нанорідини над проникною, електрично керованою поверхнею з розтягненням, вбудованою в пористе середовище. Аналіз враховує ключові фізичні ефекти, включаючи теплове випромінювання, тепловиділення, розсіювання в'язкості та хімічні реакції. Визначальні рівняння сформульовано з урахуванням впливу пористості, магнітних полів, градієнтів тепла та концентрації, а також хімічної кінетики. Особлива увага приділяється контролю об'ємної частки наночастинок на межі розділу. Для оцінки теплових характеристик розглядаються дві моделі нанорідин-мідь-вода (Cu–H_2O) та оксид алюмінію–вода (Al_2O_3–H_2O). Нелінійна крайова задача розв'язується чисельно за допомогою методу стрільби в поєднанні з методом Рунге-Кутти четвертого порядку. Результати демонструють чудову відповідність з раніше опублікованими даними, що підтверджує точність та надійність цієї моделі. Ці результати мають потенційне застосування в передових системах теплопередачі, таких як технології охолодження та обробка матеріалів.

Ключові слова: *гібридні нанорідини; МГД; пористі середовища; теплове випромінювання; поверхневе тертя*